crystals

MDPI

Article

Additive-Assisted Crystallization of 9,10-Diphenylanthracene

Alina A. Sonina [1,2], Darya S. Cheshkina [1] and Maxim S. Kazantsev [1,*]

[1] Organic Electronics Laboratory, N.N. Vorozhtsov Novosibirsk Institute of Organic Chemistry SB RAS, Lavrentiev Ave. 9, Novosibirsk 630090, Russia; belalina04@gmail.com (A.A.S.); dasha.cheshkina@yandex.ru (D.S.C.)

[2] Solid State Chemistry Department, Faculty of Natural Sciences, Novosibirsk State University, Pirogova 2, Novosibirsk 630090, Russia

* Correspondence: maximkazantsev1988@gmail.com

Abstract: Crystallization control of organic conjugated small molecules is in high demand for the engineering of functional materials in organic optoelectronics. Here, we report solution additive-assisted crystallization of a model non-planar aromatic hydrocarbon derivative 9,10-diphenylanthracene. Among the studied series of related aromatic hydrocarbons comprising pyrene, perylene, anthracene, tetracene, and rubrene, only tetracene revealed clear reproducible effects allowing one to perform selective crystallization of metastable 9,10-diphenylanthracene polymorphs. Additionally, crystallization of 9,10-diphenylanthracene and pyrene produced a stoichiometric co-crystal (PYR–DPA) having a segregated layered molecular packing with alternating 9,10-diphenylanthracene and pyrene layers. Remarkably, the molecular packing of pyrene within the co-crystal is unique and represented by the herringbone motif, whereas the molecular packing in known pyrene polymorphs is represented by π-stacked molecules. The co-crystal also demonstrated a bright photoluminescence with a photoluminescence quantum yield of 51%. Considering the morphology of 9,10-diphenylanthracene crystals obtained and crystal structures of PYR–DPA co-crystal and tetracene, we have proposed the mechanism of additive-assisted polymorphism based on the inhibition of (111) facet of α-DPA and promoting of the layered structure crystallization corresponding to metastable polymorphs (β- and γ-DPA). We highlight the additive-assisted crystallization approach as a powerful tool for the crystal engineering of functional materials for organic optoelectronics.

Keywords: additive-assisted crystallization; polymorphism; conjugated small molecules; organic semiconductors; organic electronics

check for updates

Citation: Sonina, A.A.; Cheshkina, D.S.; Kazantsev, M.S. Additive-Assisted Crystallization of 9,10-Diphenylanthracene. *Crystals* **2023**, *13*, 861. https://doi.org/10.3390/cryst13060861

Academic Editor: Ana M. Garcia-Deibe

Received: 22 April 2023
Revised: 16 May 2023
Accepted: 22 May 2023
Published: 24 May 2023

Copyright: © 2023 by the authors. Licensee MDPI, Basel, Switzerland. This article is an open access article distributed under the terms and conditions of the Creative Commons Attribution (CC BY) license (https://creativecommons.org/licenses/by/4.0/).

1. Introduction

Conjugated small molecules are well-known and widely studied molecular semiconductors. Their crystalline solids obtained both from solution and vapor or melt phases are in high demand in organic optoelectronics for possible practical applications in organic light-emitting devices, photovoltaic cells, field-effect transistors, lasers, etc. [1–4]. Among the variety of conjugated small molecules, symmetric aromatic hydrocarbon derivatives represent a convenient model for the fundamental study of "structure–property" relationships due to their condensed π-systems, known molecular packing extracted from X-ray data, low concentration of defects, and hence, outstanding charge carrier mobility and luminescent properties [5–7]. To tune a crystalline structure of organic semiconductors, several approaches were suggested and extensively exploited: variation of a conjugated framework [8–11], introduction of substituents [12–17], polymorphism [18–23], co-crystallization [24–28], template-induced [4,29–31] and specific crystallizations [22,32–36] allowing the control of crystal orientation on a substrate, and morphology. Polymorphism is considered to be one of the most powerful approaches in material science and pharmaceutical engineering for the study of "structure–activity" relationships and control of the

properties of a given compound without changing its chemical structure [37–39]. Therefore, the development of efficient crystallization approaches is in high demand in current material science.

Additive-assisted crystallization is among the most efficient approaches allowing one to regulate polymorphism and performance without time- and effort-consuming chemical synthesis [30,40–42]. Tailor-made additives were previously reported to be active promoters/inhibitors for crystallization of bio-active and pharmaceutical compounds [43–47]. The influence of even minute amounts of impurities was demonstrated to affect the kinetics and thermodynamics of a crystallization process [45]. The additives are believed to be able to bind at a certain crystal facet and impede/promote the growth of this facet. To some extent, additive-assisted crystallization is similar to template-induced crystallization and has an influence on surface chemistry, topography, and epitaxy during the nucleation process [4]. The additive-assisted crystallization of conjugated small molecules is rarely studied in material science and only a few examples were previously reported and analyzed [48]. We have previously reported additive-assisted crystallization of perylene (PRN), and the underlying mechanism was proposed based on the assumption that the 9,10-diphenylanthracene (DPA) layer serves as a template for perylene β-polymorph nucleation [24]. However, DPA itself also has three polymorphs differing by molecular packing, crystal morphologies and intermolecular interactions. Therefore, DPA may serve as a perfect platform for the study of its crystallization and further development of the crystal engineering approaches for tuning material structure and functionalities.

In this work, to demonstrate the generality of the additive-assisted crystallization method, we have studied DPA crystallization as a model non-planar luminescent aromatic hydrocarbon material being a widely used model compound in organic optoelectronics. DPA was crystallized from solution by solvent/antisolvent method with the addition of pyrene (PYR), perylene (PRN), anthracene (ANT), tetracene (TET), and rubrene (RUB). Only the tetracene additive was demonstrated to influence the DPA polymorphism allowing reproducible obtaining metastable β- and γ-DPA polymorphs, whereas the crystallization with other additives results in the thermodynamically stable α-polymorph as a major component. In addition, the crystallization of DPA and PYR allows us to obtain a stoichiometric PYR–DPA co-crystals having a segregated layered molecular packing with alternating DPA and PYR layers. The co-crystal demonstrated good photoluminescent properties with a photoluminescence quantum yield of 51%. The similarity of the α-DPA layer structure with the co-crystal structure as well as matching layer heights of β- and γ-DPA with TET molecular length allows us to propose the mechanism of additive-assisted DPA polymorphism.

2. Materials and Methods

All compounds were purchased from commercial sources (Sigma-Aldrich, Rahway, NJ, USA; Acros Organics, Geel, Belguim; Alfa Aesar, Haverhill, MA, USA; Merck, Rahway, NJ, USA). The powders were purified by the physical vapor transport method in a stream of high-purity helium (99.95%) as described elsewhere [49]. Target samples were crystallized by solvent vapor diffusion method from toluene/iPrOH system at room temperature and in dark conditions. Vials with DPA solution with or without additives in 3–5 mol% concentrations with respect to DPA in toluene were placed into a larger vessel with antisolvent (iPrOH). The DPA concentration in all experiments was 0.06 M. The crystal growth time was about 3 days. Crystals were examined using an optical microscope (MC-2-Zoom (2CR), "Micromed", Russia) in transmitted light and under blue (405 nm) irradiation.

2.1. X-ray Diffraction

Single-crystal X-ray diffraction experiments were performed using a Bruker KAPPA APEX II diffractometer with graphite monochromated MoKα radiation at ambient temperature. Integration and scaling of the intensity data were accomplished with SAINT [50]. Absorption corrections were applied using SADABS [51]. The structure was solved by

SHELXT [52]. Refinement was carried out by the full-matrix least-squares technique with SHELXL [52] using OLEX2 [53] software. All non-hydrogen atoms were refined anisotropically. Hydrogen atoms were calculated at idealized positions according to the riding model. Parameters characterizing data collection, refinement, and crystal data of PYR–DPA co-crystal are summarized in Table S1 (see Supplementary Materials). Mercury [54] Olex2 and PLATON [55] were used for visualization and analysis of the crystal structure. The structural data for the co-crystal was deposited at the Cambridge Crystallographic Database (CCDC No. 2254697) and can be downloaded freely from the following site: http://www.ccdc.cam.ac.uk. The theoretical morphology was calculated using Bravais–Friedel–Donnay–Harker (BFDH) method in Mercury.

Powder X-ray diffraction experiments were performed using a STOE-MP diffractometer (Cu Kα radiation), equipped with a bent Ge (111) monochromator and a MYTHEN 1 K detector, scanning a 2θ range of 4–50°. The experimental powder pattern of the samples was compared with those simulated form the single-crystal X-ray diffraction data of previously reported polymorphs taken from the Cambridge Structural Database. For qualitative phase analyses, the published CIFs of DPA polymorphs have been chosen at ambient temperature and better R_f (<5%) values according to the following refs: α-DPA (CSD-DPANTR01) [56], β-DPA (CSD-DPANTR08) [57], γ-DPA (CSD-DPANTR11) [57]. Crystal structure of tetracene (CSD-TETCEN01) [58] and perylene-9,10-diphenylanthacene (PRN-DPA) co-crystal (CSD-QIFKAV) [24] were used for crystal packing comparison with polymorphic forms of DPA.

2.2. Photoluminescence Measurements

The photoluminescence quantum yield of single crystals was measured using an in-tegrating sphere 3.3-inch-diameter (Newport 819C-SL-3.3) coupled with a UV-Vis spectrometer (QE Pro, Ocean Optics). The excitation was performed with a diode laser emitting 405 nm (Laserglow). The detailed experimental procedure is described in ref. [59]. All samples showed good reproducibility and the overall error did not exceed 4%.

3. Results and Discussion

3.1. Additive-Assisted Crystallization of 9,10-Diphenylanthracene

9,10-diphenylanthracene (DPA) was previously reported to have three polymorphic modifications: α-, β-, and γ-polymorphs differing by molecular packing and crystal morphology. The α-form was demonstrated to be thermodynamically stable, whereas the metastable β- and γ-forms demonstrated similar unit cell parameters but different crystal structures and are often obtained as a mixture from sublimation or from melt [57]. DPA has 14 deposited crystal structures according to the last CSD version 5.43. We analyzed all deposited structures and assigned them to the three DPA polymorphs as follows: α-DPA (refcodes: DPANTR, DPANTR01, DPANTR03-06, and DPANTR13), β-DPA (refcode DPANTR08-10), and γ-DPA (refcode DPANTR02,11). All CSD numbers relating to one polymorphic form have similar powder patterns simulated from CIF files. However, the structure with refcode DPANTR07 (3 GPa) [60] was reported to have slightly different unit cell parameters (10.041(2) Å, 13.150(2) Å, 11.378(2) Å, 90°, 88.48(1)°, 90°) and powder pattern as compared to that of α-DPA. We analyzed DPANTR01 and DPANTR07 for structural similarities and concluded that these crystal structures are very similar: all 15 molecules in the cluster overlay with each other with a slight shift and RMS = 0.509. Therefore, this phase can hardly be considered to be a new DPA polymorph but rather a compressed structure of α-DPA.

To study 9,10-diphenylanthracene polymorphism, we crystallized it by solvent/antisolvent method with the following conjugated hydrocarbon molecules as additives: pyrene (PYR), perylene (PRN), anthracene (ANT), tetracene (TET), and rubrene (RUB) (Chart 1). Additive molecules were chosen from the same class—conjugated small molecules with different molecular length and width, crystal packing, and molecular planarity. Thermodynamically

stable α-polymorph of DPA was typically obtained from toluene solution with i-PrOH as an antisolvent (without additives).

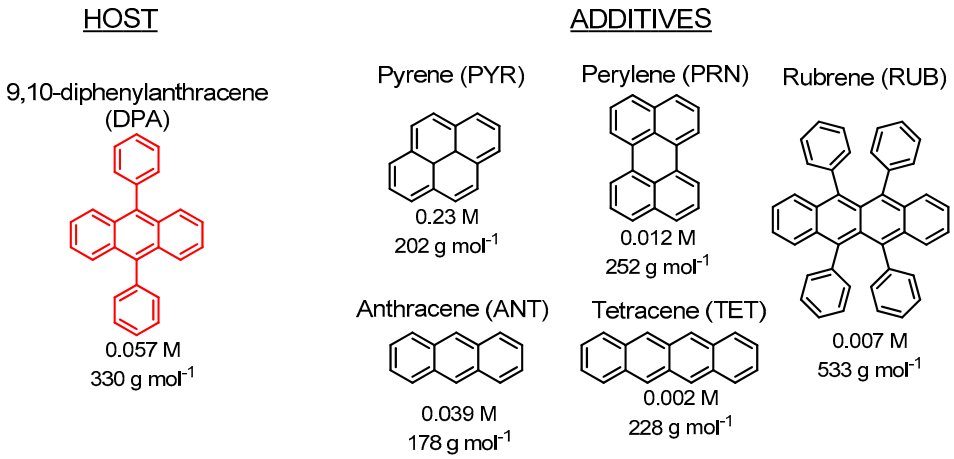


Chart 1. Chemical structures of 9,10-diphenylanthracene and additives with their molecular weight and estimated solubility in toluene.

Figure 1a–e shows the optical images of DPA crystals grown in the presence of additives. Typically, DPA crystallizes from a toluene–iPrOH system as bulk crystals with prism morphology (Figure 1a). Crystallization with certain additives (PYR, PRN and RUB) led to thick plate crystals (Figure 1b,c,e). The Miller indexing of the DPA plate-shaped crystals shows that the main crystal facet is (111), which corresponds to the inclined molecular arrangement in respect the main crystal facet (Figure 1f). Crystallization of DPA with PYR, PRN, and RUB did not lead to polymorphic diversity of DPA (Figures 1 and 2). The crystallization of DPA with anthracene results in the concomitant polymorphism of α- and β-forms of DPA, according to powder X-ray diffraction experiments (Figure 2 and Figure S1). PXRD patterns of DPA + ANT mixtures (Figure S1) demonstrated a large contribution of α-polymorph; the β-form was observed only as a minor product, even at high ANT concentrations (up to 20%).

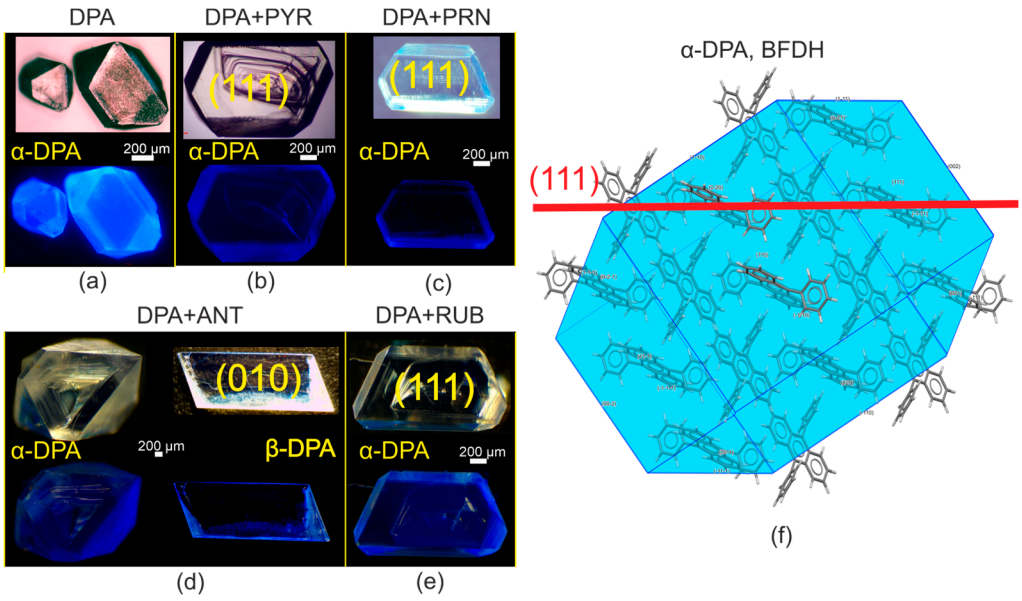


Figure 1. Optical microscopy images of DPA crystals (**a**) pure and obtained with additives: (**b**) DPA + PYR, (**c**) DPA + PRN, (**d**) DPA + ANT, and (**e**) DPA + RUB in transmitted light (top) and under blue irradiation (bottom); (**f**) BFDH morphology of α-DPA with (111) slice.

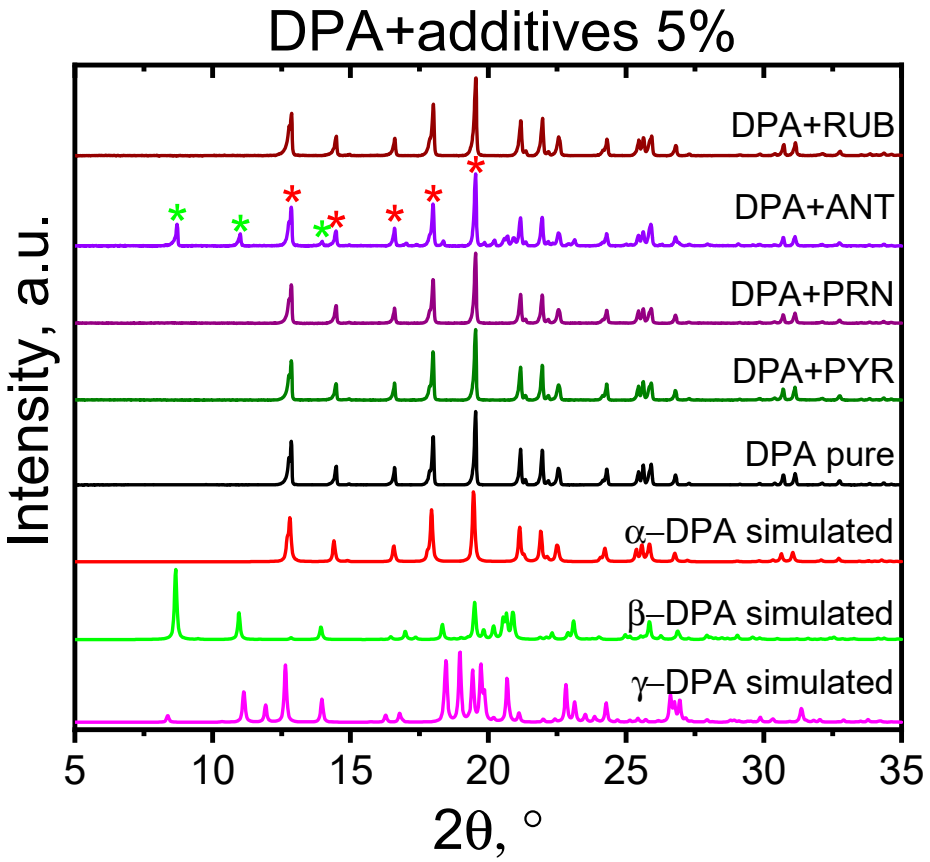


Figure 2. The powder X-ray diffraction data of DPA polymorphs simulated from single-crystal X-ray diffraction data of α-form (red), β-form (green), and γ-form (magenta) in comparison with experimental data of the samples crystallized with additives (PYR, PRN, ANT, RUB). The asterisks with matching colors demonstrate the peaks related to α- and β-DPA.

More intriguing results were obtained in the case of using tetracene as an additive. The variation of tetracene concentration reproducibly allows us to obtain all three known polymorphic forms of DPA as follows. Crystallization of DPA with the presence of tetracene in concentrations lower than 1% retains the crystal form of α-DPA but changes crystal morphology from bulk prisms to plates with (111) main facets (Figure 3a). Using near-saturated tetracene concentrations (up to 3%) results in plate-like DPA crystals corresponding to β- and γ-metastable forms of DPA (Figure 3b,c). The powder X-ray diffraction confirmed the selective crystallization of DPA polymorphic forms (Figure 3d). Figure S2 shows powder patterns of a series of DPA+TET samples crystallized with different TET concentrations (at least 3 PXRD experiments for each TET concentration were performed) indicating a good reproducibility of TET-assisted DPA crystallization. The mechanism of the tetracene effect probably could have been rationalized by obtaining a DPA–TET co-crystal and analyzing its structure. However, during crystallization experiments even with saturated concentrations of DPA and TET and even by using a physical vapor transport method it was not obtained. We also tried a mechanochemical approach to obtain a possible DPA–TET co-crystal phase. The stoichiometric mixture of DPA and TET was ground with a drop of toluene in an agate mortar and PXRD pattern was recorded (Figure S3). However, only peaks of individual phases of both materials (α-DPA and TET) were observed. Nevertheless, during the study, a new co-crystal of DPA with PYR was obtained and is characterized in the following section.

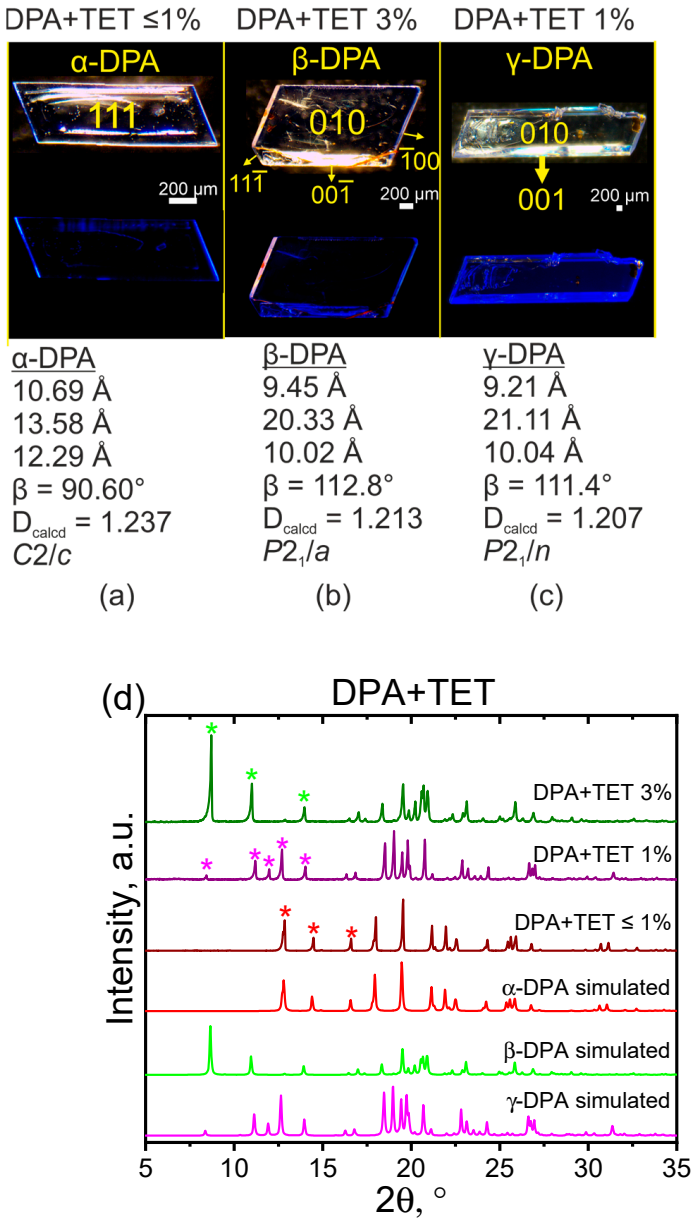


Figure 3. (**a**–**c**) Optical microscopy images of DPA with different tetracene concentrations in transmitted light (top) and under blue irradiation (bottom). (**d**) The powder X-ray diffraction data of DPA with tetracene. The asterisks with matching colors demonstrate the peaks related to the α- (red), β- (green), and γ-DPA (magenta) polymorphs.

3.2. Co-Crystal of Pyrene and 9,10-Diphenylanthracene (PYR–DPA)

PYR–DPA co-crystal was observed as a minor product at crystallization of DPA with pyrene in concentration of 5 mol%. Co-crystal has rhombic plate-like morphology with blue photoluminescence predominantly emitted from the crystal edges under blue irradiation (Figure 4a). The main crystal facet of the co-crystal is (100) plane that corresponds to BFDH-calculated morphology (Figure 4a). The PYR–DPA co-crystal crystallized in a monoclinic $P2_1/c$ space group with halves of molecules in asymmetric units (Figure 4b). PYR and DPA pack in layered structures with alternating of their layers. DPA layers implemented by C-H···π interactions (C_4-H···Cg^2 and C_5-H···Cg^1) between anthracene cores (Table S2, Figure 4b). PYR and DPA layers connected by C_{10}-H···Cg^5 and C_{11}-H···Cg^6 interactions between phenyl groups and PYR core (Table S2, Figure 4b). PYR layers have herringbone packing with weak C-H···π interactions, where H···Cg distance is longer than 3.4 Å.

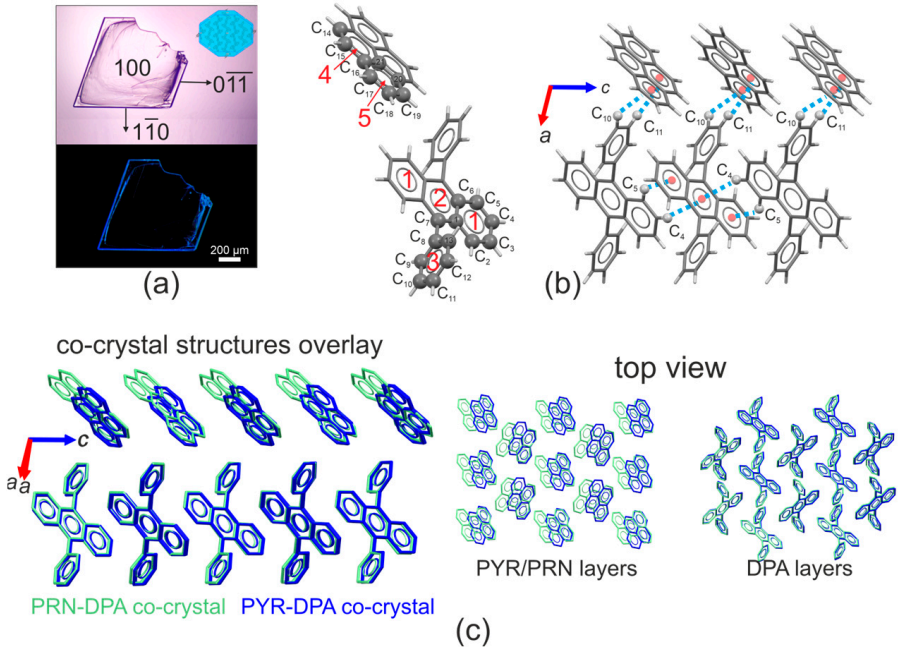


Figure 4. (**a**) Optical images of the PYR–DPA co-crystal in transmitted light (top) and under blue irradiation (bottom) with calculated BFDH morphology. (**b**) Molecular structure, atom, and cycle numbering and C-H···π interactions of the PYR–DPA co-crystal. (**c**) Comparison of crystal structures of PYR–DPA (blue) and PRN–DPA (green) co-crystals with side and top view.

Remarkably, the co-crystal is isostructural to the previously reported PRN–DPA co-crystal (refcode: CSD-QIFKAV, Figure 4c). Co-crystal structures have the same space group $P2_1/c$ and similar unit cell parameters. The arrangement of DPA molecules in co-crystals is identical, see top view in Figure 4c. The pyrene/perylene layers have similar inclination and herringbone packing stabilized by C-H···π interactions with DPA layers. However, weaker C-H···π interactions in pyrene layers make the packing less dense than that of PRN–DPA co-crystal with D_{calcd} = 1.237 versus D_{calcd} = 1.267 g cm^{-3} for PRN–DPA co-crystal. Weaker C-H···π interactions in pyrene layers may be related to unfavorable herringbone packing, because in all three known polymorphs of PYR the π-stacking is realized—this is consistent with the photoluminescence properties of studied PYR and PYR–DPA materials (vide infra). This result might also be attractive for template crystallization of new polymorphic forms of pyrene with herringbone packing.

As a next step, we studied the photoluminescence (PL) properties of the PYR–DPA co-crystal as well as PYR and DPA crystals by integrating sphere. Figure 5 demonstrates corresponding PL spectra normalized to PL QY. α-DPA demonstrated a PL spectrum with maxima at 450 nm and PL QY of 23%. The pyrene polycrystalline sample obtained from toluene solution demonstrated a broad PL spectrum with maxima at about 500 nm and similar to DPA PL QY of 23%, which is lower than the previously reported value of 68% for melt-grown PYR crystals [61] and in accordance with previous report on PL properties of methylated PYR derivatives [61]. The relatively low PL QY of the solution-crystallized PYR sample may be assigned to the defects and dense π-π stacked molecular packing leading to excimer formation in the solid state. However, PYR–DPA co-crystal demonstrated a blue-shifted emission with two PL maxima at 431 nm and 453 nm with a high PL QY of 51%, which could be assigned to the less dense crystal structure and non-typical herringbone packing of PYR molecules within the co-crystal (vide supra). The PL QY of PYR–DPA co-crystal is also consistent with its isostructural analogue PRN–DPA co-crystal demonstrating a PLQY of 45% [24].

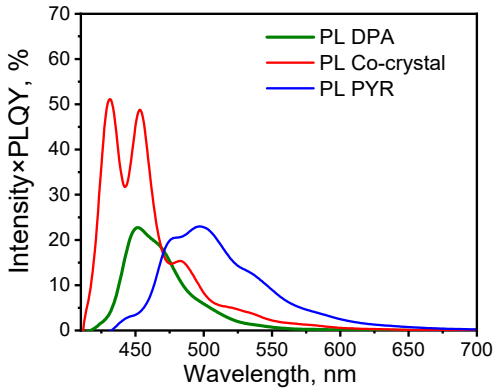


Figure 5. PL spectra normalized to PL QY of α-DPA crystals (olive), PYR polycrystalline sample (blue), and PYR–DPA co-crystal (red).

3.3. 9,10-Diphenylanthracene Polymorphism Control

Crystallization of DPA with additives changes DPA crystal morphology from bulk prisms to plate-shaped crystals with (111) Miller indexes. This observation points on the inhibiting of the growth of (111) facet. Additionally, similar crystal structures of PRN-DPA and PYR–DPA co-crystals point to preferential DPA layered packing during a crystallization process due to the difference between DPA and additive molecular structure [25]. We compared DPA arrangement of (111) layer in α-DPA and PYR–DPA co-crystal to discover possible similarities. Crystal structure comparison shows the similar molecular arrangement of molecular stacks of the α-DPA (111) layer and PYR–DPA co-crystal (100) layer (see side and top view of DPA layer in Figure 6a; highlighted by red circles). Such an arrangement of DPA molecules allows them to form stronger C-H···π interactions with additive inhibiting further growth of the (111) layer and the changing crystal morphology to the plate. We supposed that the (111) DPA layer serves as adsorption layer for tetracene molecules that incorporate into the DPA layers and are able to transform not only the crystal morphology but also the polymorphic modification via changing molecular arrangement to the layered structure (Figure 6a) corresponding to β- or γ- DPA polymorphs. Figure 6b–e demonstrates the comparison of the molecular layer thickness with the tetracene molecular length indicating very similar values. Therefore, the tetracene additive most probably acts as a promoter for layered DPA crystallization corresponding to β- and γ-DPA polymorphs.

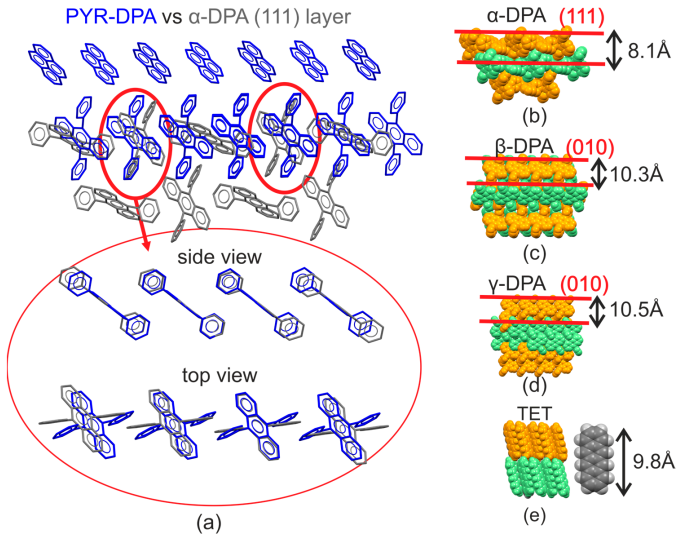


Figure 6. (**a**) Comparison of (111) layer in α-DPA (grey) with (100) DPA layer of PYR–DPA co-crystals (blue). The red circles show similar fragments. (**b**–**e**) Molecular packing and layer height of DPA polymorphic forms' and tetracene. The orange and green color highlight alternating molecular layers.

4. Conclusions

In summary, we have demonstrated the additive-assisted crystallization of 9,10-diphenylanthracene from solution by solvent/antisolvent method. The series of model aromatic hydrocarbon molecules comprising pyrene, perylene, anthracene, tetracene, and rubrene was tested for polymorphism control of DPA. All materials except anthracene and tetracene did not demonstrate unambiguous influence on DPA polymorphism. In turn, tetracene showed a reproducible effect on the metastable DPA polymorphs' crystallization allowing us to obtain α-, β-, and γ-DPA polymorph depending on the TET concentration that was demonstrated for the first time. In addition, the crystallization of DPA and PYR resulted in stoichiometric PYR–DPA co-crystal having a segregated layered molecular packing with alternating DPA and PYR layers. The segregated structure of the PYR–DPA co-crystal highlights the molecular incompatibility of non-planar and planar aromatic hydrocarbon molecules for the mixed co-crystallization [25]. Remarkably, the molecular packing of pyrene within the co-crystal is unique and represented by the herringbone motif, whereas the molecular packing in known pyrene polymorphs is denser and represented by π-stacked molecules. The co-crystal demonstrated bright photoluminescence with a photoluminescence quantum yield of 51%. Finally, considering the TET molecular length, DPA polymorphs' structures and the PYR–DPA and PRN–DPA [24] co-crystals' structures, we have proposed the mechanism of additive-assisted DPA polymorphism based on the promotion of the segregated layered crystallization corresponding to metastable DPA polymorphs. Our work highlights the additive-assisted crystallization method for tuning of molecular packing and functional properties of materials for organic optoelectronics.

Supplementary Materials: The following supporting information can be downloaded at: https://www.mdpi.com/article/10.3390/cryst13060861/s1, Table S1: Crystal Data of PYR-DPA co-crystal; Figure S1: Powder X-ray diffraction patterns of DPA + ANT samples at different ANT concentrations; Figure S2: A series of powder X-ray diffraction patterns of DPA + TET samples with variable TET concentrations; Figure S3: Powder X-ray diffraction patterns of DPA + TET mixture after mechanochemical treatment; Table S2: Noncovalent interactions in PYR-DPA co-crystal.

Author Contributions: Conceptualization, writing—original draft preparation, A.A.S. and M.S.K.; methodology, validation, formal analysis, investigation, resources, data curation, visualization, project administration, funding acquisition, A.A.S.; investigation optical properties, D.S.C.; writing—review and editing, supervision, M.S.K. All authors have read and agreed to the published version of the manuscript.

Funding: This work was supported by the Russian Science Foundation, project 21-73-00287.

Data Availability Statement: Not applicable.

Acknowledgments: Powder diffraction experiments were performed using the equipment of the laboratory "Molecular Design and Ecologically Safe Technologies" at the Novosibirsk State University. The assistance of E.A. Losev is gratefully acknowledged.

Conflicts of Interest: The authors declare no conflict of interest.

References

1. Peng, Z.; Stingelin, N.; Ade, H.; Michels, J.J. A materials physics perspective on structure–processing–function relations in blends of organic semiconductors. *Nat. Rev. Mater.* **2023**, 1–17. [CrossRef]
2. Chen, J.; Zhang, W.; Wang, L.; Yu, G. Recent Research Progress of Organic Small-Molecule Semiconductors with High Electron Mobilities. *Adv. Mater.* **2023**, *35*, e2210772. [CrossRef] [PubMed]
3. Xu, C.; Zhao, Z.; Yang, K.; Niu, L.; Ma, X.; Zhou, Z.; Zhang, X.; Zhang, F. Recent progress in all-small-molecule organic photovoltaics. *J. Mater. Chem. A* **2022**, *10*, 6291–6329. [CrossRef]
4. Parambil, J.V.; Poornachary, S.K.; Heng, J.Y.Y.; Tan, R.B.H. Template-induced nucleation for controlling crystal polymorphism: From molecular mechanisms to applications in pharmaceutical processing. *CrystEngComm* **2019**, *21*, 4122–4135. [CrossRef]
5. Zhang, X.; Dong, H.; Hu, W. Organic Semiconductor Single Crystals for Electronics and Photonics. *Adv. Mater.* **2018**, *30*, e1801048. [CrossRef]

6. Podzorov, V. Organic single crystals: Addressing the fundamentals of organic electronics. *MRS Bull.* **2013**, *38*, 15–24. [CrossRef]
7. Zaumseil, J.; Sirringhaus, H. Electron and ambipolar transport in organic field-effect transistors. *Chem. Rev.* **2007**, *107*, 1296–1323. [CrossRef]
8. Parashchuk, O.D.; Mannanov, A.A.; Konstantinov, V.G.; Dominskiy, D.I.; Surin, N.M.; Borshchev, O.V.; Ponomarenko, S.A.; Pshenichnikov, M.S.; Paraschuk, D.Y. Molecular Self-Doping Controls Luminescence of Pure Organic Single Crystals. *Adv. Funct. Mater.* **2018**, *28*, 1800116. [CrossRef]
9. Kazantsev, M.S.; Beloborodova, A.A.; Kuimov, A.D.; Koskin, I.P.; Frantseva, E.S.; Rybalova, T.V.; Shundrina, I.K.; Becker, C.S.; Mostovich, E.A. Synthesis, luminescence and charge transport properties of furan/phenylene co-oligomers: The study of conjugation length effect. *Org. Electron.* **2018**, *56*, 208–215. [CrossRef]
10. Komori, T.; Nakanotani, H.; Yasuda, T.; Adachi, C. Light-emitting organic field-effect transistors based on highly luminescent single crystals of thiophene/phenylene co-oligomers. *J. Mater. Chem. C* **2014**, *2*, 4918–4921. [CrossRef]
11. Hotta, S.; Yamao, T. The thiophene/phenylene co-oligomers: Exotic molecular semiconductors integrating high-performance electronic and optical functionalities. *J. Mater. Chem.* **2011**, *21*, 1295–1304. [CrossRef]
12. Park, W.; Yun, C.; Yun, S.; Lee, J.-J.; Bae, S.; Ho, D.; Kim, C.; Seo, S. Effects of alkyl chain on the liquid crystalline properties of [1]benzothieno[3,2-b][1]benzothiophene-based organic semiconductors. *Org. Electron.* **2022**, *105*, 106508. [CrossRef]
13. Li, J.; Qin, Z.; Sun, Y.; Zhen, Y.; Liu, J.; Zou, Y.; Li, C.; Lu, X.; Jiang, L.; Zhang, X.; et al. Regulating Crystal Packing by Terminal tert-Butylation for Enhanced Solid-State Emission and Efficacious Charge Transport in an Anthracene-Based Molecular Crystal. *Angew. Chem. Int. Ed. Engl.* **2022**, *61*, e202206825. [CrossRef] [PubMed]
14. Sosorev, A.Y.; Trukhanov, V.A.; Maslennikov, D.R.; Borshchev, O.V.; Polyakov, R.A.; Skorotetcky, M.S.; Surin, N.M.; Kazantsev, M.S.; Dominskiy, D.I.; Tafeenko, V.A.; et al. Fluorinated Thiophene-Phenylene Co-Oligomers for Optoelectronic Devices. *ACS Appl. Mater. Interfaces* **2020**, *12*, 9507–9519. [CrossRef]
15. An, M.H.; Ding, R.; Zhu, Q.C.; Ye, G.D.; Wang, H.; Du, M.X.; Chen, S.N.; Liu, Y.; Xu, M.L.; Xu, T.; et al. Well-Balanced Ambipolar Organic Single Crystals toward Highly Efficient Light-Emitting Devices. *Adv. Funct. Mater.* **2020**, *30*, 2002422. [CrossRef]
16. Sosorev, A.Y.; Nuraliev, M.K.; Feldman, E.V.; Maslennikov, D.R.; Borshchev, O.V.; Skorotetcky, M.S.; Surin, N.M.; Kazantsev, M.S.; Ponomarenko, S.A.; Paraschuk, D.Y. Impact of terminal substituents on the electronic, vibrational and optical properties of thiophene-phenylene co-oligomers. *Phys. Chem. Chem. Phys.* **2019**, *21*, 11578–11588. [CrossRef] [PubMed]
17. Kazantsev, M.S.; Beloborodova, A.A.; Frantseva, E.S.; Rybalova, T.V.; Konstantinov, V.G.; Shundrina, I.K.; Paraschuk, D.Y.; Mostovich, E.A. Methyl substituent effect on structure, luminescence and semiconducting properties of furan/phenylene co-oligomer single crystals. *CrystEngComm* **2017**, *19*, 1809–1815. [CrossRef]
18. Jinjyo, T.; Mizuno, H.; Sasaki, F.; Yanagi, H. Polymorph- and molecular alignment-dependent lasing behaviors of a cyano-substituted thiophene/phenylene co-oligomer. *J. Mater. Chem. C* **2023**, *11*, 1714–1725. [CrossRef]
19. Chung, H.; Chen, S.; Patel, B.; Garbay, G.; Geerts, Y.H.; Diao, Y. Understanding the Role of Bulky Side Chains on Polymorphism of BTBT-Based Organic Semiconductors. *Cryst. Growth Des.* **2020**, *20*, 1646–1654. [CrossRef]
20. Sonina, A.A.; Koskin, I.P.; Sherin, P.S.; Rybalova, T.V.; Shundrina, I.K.; Mostovich, E.A.; Kazantsev, M.S. Crystal packing control of a trifluoromethyl-substituted furan/phenylene co-oligomer. *Acta Cryst. B* **2018**, *74*, 450–457. [CrossRef]
21. Galindo, S.; Tamayo, A.; Leonardi, F.; Mas-Torrent, M. Control of Polymorphism and Morphology in Solution Sheared Organic Field-Effect Transistors. *Adv. Funct. Mater.* **2017**, *27*, 1700526. [CrossRef]
22. Varghese, S.; Park, S.K.; Casado, S.; Resel, R.; Wannemacher, R.; Lüer, L.; Park, S.Y.; Gierschner, J. Polymorphism and Amplified Spontaneous Emission in a Dicyano-Distyrylbenzene Derivative with Multiple Trifluoromethyl Substituents: Intermolecular Interactions in Play. *Adv. Funct. Mater.* **2016**, *26*, 2349–2356. [CrossRef]
23. Chung, H.; Diao, Y. Polymorphism as an emerging design strategy for high performance organic electronics. *J. Mater. Chem. C* **2016**, *4*, 3915–3933. [CrossRef]
24. Sonina, A.A.; Kuimov, A.D.; Shumilov, N.A.; Koskin, I.P.; Kardash, T.Y.; Kazantsev, M.S. Additive-Assisted Perylene Polymorphism Controlled via Secondary Bonding Interactions. *Cryst. Growth Des.* **2023**, *23*, 2710–2720. [CrossRef]
25. Kuimov, A.D.; Becker, C.S.; Sonina, A.A.; Kazantsev, M.S. Host–guest molecular doping guide for emissive organic semiconductor crystals. *New J. Chem.* **2022**, *46*, 21257–21267. [CrossRef]
26. Campillo-Alvarado, G.; Bernhardt, M.; Davies, D.W.; Soares, J.; Woods, T.J.; Diao, Y. Modulation of pi-stacking modes and photophysical properties of an organic semiconductor through isosteric cocrystallization. *J. Chem. Phys.* **2021**, *155*, 071102. [CrossRef]
27. Zhang, J.; Gu, P.; Long, G.; Ganguly, R.; Li, Y.; Aratani, N.; Yamada, H.; Zhang, Q. Switching charge-transfer characteristics from p-type to n-type through molecular "doping" (co-crystallization). *Chem. Sci.* **2016**, *7*, 3851–3856. [CrossRef]
28. Hutchins, K.M.; Groeneman, R.H.; Reinheimer, E.W.; Swenson, D.C.; MacGillivray, L.R. Achieving dynamic behaviour and thermal expansion in the organic solid state via co-crystallization. *Chem. Sci.* **2015**, *6*, 4717–4722. [CrossRef]
29. Zhou, Q.; Lei, Y.; Fu, H. A molecular design principle towards luminescent polymorphic organic heterostructured architectures. *J. Mater. Chem. C* **2021**, *9*, 489–496. [CrossRef]
30. Levesque, A.; Maris, T.; Wuest, J.D. ROY Reclaims Its Crown: New Ways To Increase Polymorphic Diversity. *J. Am. Chem. Soc.* **2020**, *142*, 11873–11883. [CrossRef]

31. Singh, A.; Lee, I.S.; Kim, K.; Myerson, A.S. Crystal growth on self-assembled monolayers. *CrystEngComm* **2011**, *13*, 24–32. [CrossRef]
32. Metherall, J.P.; Carroll, R.C.; Coles, S.J.; Hall, M.J.; Probert, M.R. Advanced crystallisation methods for small organic molecules. *Chem. Soc. Rev.* **2023**, *52*, 1995–2010. [CrossRef] [PubMed]
33. Roche, G.H.; Flot, D.; Moreau, J.J.E.; Dautel, O.J.; Filhol, J.-S.; van der Lee, A. Packing Polymorphism Affecting the Optoelectronic Properties of a π-Conjugated Organic Compound. *Cryst. Growth Des.* **2021**, *21*, 3850–3863. [CrossRef]
34. Cruz-Cabeza, A.J.; Davey, R.J.; Sachithananthan, S.S.; Smith, R.; Tang, S.K.; Vetter, T.; Xiao, Y. Aromatic stacking—A key step in nucleation. *Chem. Commun.* **2017**, *53*, 7905–7908. [CrossRef] [PubMed]
35. Diao, Y.; Shaw, L.; Bao, Z.; Mannsfeld, S.C.B. Morphology control strategies for solution-processed organic semiconductor thin films. *Energy Environ. Sci.* **2014**, *7*, 2145–2159. [CrossRef]
36. Liu, C.; Minari, T.; Li, Y.; Kumatani, A.; Lee, M.V.; Athena Pan, S.H.; Takimiya, K.; Tsukagoshi, K. Direct formation of organic semiconducting single crystals by solvent vapor annealing on a polymer base film. *J. Mater. Chem.* **2012**, *22*, 8462–8469. [CrossRef]
37. Cruz-Cabeza, A.J.; Feeder, N.; Davey, R.J. Open questions in organic crystal polymorphism. *Commun. Chem.* **2020**, *3*, 142. [CrossRef]
38. Brog, J.-P.; Chanez, C.-L.; Crochet, A.; Fromm, K.M. Polymorphism, what it is and how to identify it: A systematic review. *RSC Adv.* **2013**, *3*, 16905–16931. [CrossRef]
39. Mangin, D.; Puel, F.; Veesler, S. Polymorphism in Processes of Crystallization in Solution: A Practical Review. *Org. Process Res. Dev.* **2009**, *13*, 1241–1253. [CrossRef]
40. Shtukenberg, A.G.; Lee, S.S.; Kahr, B.; Ward, M.D. Manipulating crystallization with molecular additives. *Annu. Rev. Chem. Biomol. Eng.* **2014**, *5*, 77–96. [CrossRef]
41. Song, R.-Q.; Cölfen, H. Additive controlled crystallization. *CrystEngComm* **2011**, *13*, 1249–1276. [CrossRef]
42. Weissbuch, I.; Popovitz-Biro, R.; Lahav, M.; Leiserowitz, L. Understanding and control of nucleation, growth, habit, dissolution and structure of two- and three-dimensional crystals using 'tailor-made' auxiliaries. *Acta Crystallogr. Sect. B* **1995**, *51*, 115–148. [CrossRef]
43. Sun, J.; Wang, Y.; Gao, Z.; Gong, J.; Tang, W. Additive-assisted preferential crystallization of racemic component: A case of norvaline. *J. Ind. Eng. Chem.* **2022**, *110*, 206–216. [CrossRef]
44. Shtukenberg, A.G.; Ward, M.D.; Kahr, B. Crystal growth inhibition by impurity stoppers, now. *J. Cryst. Growth.* **2022**, *597*, 126839. [CrossRef]
45. Xu, S.; Cao, D.; Liu, Y.; Wang, Y. Role of Additives in Crystal Nucleation from Solutions: A Review. *Cryst. Growth Des.* **2021**, *22*, 2001–2022. [CrossRef]
46. Losev, E.A.; Mikhailenko, M.A.; Achkasov, A.F.; Boldyreva, E.V. The effect of carboxylic acids on glycine polymorphism, salt and co-crystal formation. A comparison of different crystallisation techniques. *New J. Chem.* **2013**, *37*, 1973–1981. [CrossRef]
47. Weissbuch, I.; Leiserowitz, L.; Lahav, M. Direct assignment of the absolute configuration of molecules from crystal morphology. *Chirality* **2008**, *20*, 736–748. [CrossRef]
48. Sonina, A.A.; Becker, C.S.; Kuimov, A.D.; Shundrina, I.K.; Komarov, V.Y.; Kazantsev, M.S. Alkyl-substituted bis(4-((9H-fluoren-9-ylidene)methyl)phenyl)thiophenes: Weakening of intermolecular interactions and additive-assisted crystallization. *CrystEngComm* **2021**, *23*, 2654–2664. [CrossRef]
49. de Boer, R.W.I.; Gershenson, M.E.; Morpurgo, A.F.; Podzorov, V. Organic single-crystal field-effect transistors. *Phys. Status Solidi A* **2004**, *201*, 1302–1331. [CrossRef]
50. *SAINT*; Data Reduction and Frame Integration Program for the CCD Area-Detector System; Bruker Analytical X-ray Systems: Madison, WI, USA, 2006.
51. Sheldrick, G.M. *SADABS*; Institute for Inorganic Chemistry, University of Goettingen: Goettingen, Germany, 1996.
52. Sheldrick, G.M. Crystal structure refinement with SHELXL. *Acta Crystallogr. Sect. C* **2015**, *71*, 3–8. [CrossRef]
53. Dolomanov, O.V.; Bourhis, L.J.; Gildea, R.J.; Howard, J.A.K.; Puschmann, H. OLEX2: A complete structure solution, refinement and analysis program. *J. Appl. Crystallogr.* **2009**, *42*, 339–341. [CrossRef]
54. Macrae, C.F.; Edgington, P.R.; McCabe, P.; Pidcock, E.; Shields, G.P.; Taylor, R.; Towler, M.; van de Streek, J. Mercury: Visualization and analysis of crystal structures. *J. Appl. Cryst.* **2006**, *39*, 453–457. [CrossRef]
55. Spek, A.L. Structure validation in chemical crystallography. *Acta Cryst. D* **2009**, *65*, 148–155. [CrossRef] [PubMed]
56. Langer, V.; Becker, H.D. Crystal structure of 9,10-diphenylanthracene, (C6H5)(C14H8)(C6H5). *Z. Krist.-Cryst. Mater.* **1992**, *199*, 313–315. [CrossRef]
57. Salzillo, T.; Della Valle, R.G.; Venuti, E.; Brillante, A.; Siegrist, T.; Masino, M.; Mezzadri, F.; Girlando, A. Two New Polymorphs of the Organic Semiconductor 9,10-Diphenylanthracene: Raman and X-ray Analysis. *J. Phys. Chem. C* **2016**, *120*, 1831–1840. [CrossRef]
58. Holmes, D.; Kumaraswamy, S.; Matzger, A.J.; Vollhardt, K.P.C. On the Nature of Nonplanarity in the [N]Phenylenes. *Chem. Eur. J.* **1999**, *5*, 3399–3412. [CrossRef]
59. Kazantsev, M.S.; Frantseva, E.S.; Kudriashova, L.G.; Konstantinov, V.G.; Mannanov, A.A.; Rybalova, T.V.; Karpova, E.V.; Shundrina, I.K.; Kamaev, G.N.; Pshenichnikov, M.S.; et al. Highly-Emissive Solution-Grown Furan/Phenylene Co-Oligomer Single Crystals. *RSC Adv.* **2016**, *6*, 92325–92329. [CrossRef]

60. Fabbiani, F.P.A.; Bergantin, S.; Gavezzotti, A.; Rizzato, S.; Moret, M. X-ray diffraction and computational studies of the pressure-dependent tetrachloroethane solvation of diphenylanthracene. *CrystEngComm* **2016**, *18*, 2173–2181. [CrossRef]
61. Katoh, R.; Suzuki, K.; Furube, A.; Kotani, M.; Tokumaru, K. Fluorescence Quantum Yield of Aromatic Hydrocarbon Crystals. *J. Phys. Chem. C* **2009**, *113*, 2961–2965. [CrossRef]

Disclaimer/Publisher's Note: The statements, opinions and data contained in all publications are solely those of the individual author(s) and contributor(s) and not of MDPI and/or the editor(s). MDPI and/or the editor(s) disclaim responsibility for any injury to people or property resulting from any ideas, methods, instructions or products referred to in the content.